



# Modification of midlatitude ionospheric parameters in the F2 layer by persistent high-speed solar wind streams

M. H. Denton,<sup>1</sup> T. Ulich,<sup>2</sup> and E. Turunen<sup>2</sup>

Received 22 September 2008; revised 23 January 2009; accepted 5 February 2009; published 23 April 2009.

[1] High-speed solar wind streams (HSSs) are periods of persistently high solar wind, which emanate from coronal holes and may recur with a frequency related to the solar rotation period of 27 days. On arrival at the Earth's magnetopause, such streams cause a series of events which ultimately lead to changes in the ionospheric F layer. We present a superposed epoch analysis of parameters in the midlatitude F2 layer for a collection of 124 high-speed solar wind streams which occurred between 1993 and 2006. Clear changes in the critical frequency (foF2), density (NmF2), and height (hmF2) are found to occur after the onset of magnetospheric convection associated with HSS arrival at the Earth's magnetosphere. A fall in foF2 occurs immediately following convection onset accompanied by a sudden decrease in NmF2 and an increase in hmF2. During the events under study, the height of the F2 layer is found to increase by  $\sim 20$  km at convection onset. A period of more than 4 days is required for the ionosphere to return to preevent levels. This behavior is explained as the occurrence of ionospheric F region storms following HSS arrival. The results raise the possibility of improved predictions for ionospheric parameters on the basis of upstream solar wind conditions and prior identification of stream interfaces.

**Citation:** Denton, M. H., T. Ulich, and E. Turunen (2009), Modification of midlatitude ionospheric parameters in the F2 layer by persistent high-speed solar wind streams, *Space Weather*, 7, S04006, doi:10.1029/2008SW000443.

## 1. Introduction

[2] A quasi-27-day periodicity in various atmospheric, ionospheric, and magnetospheric parameters has previously been reported in numerous studies, some dating to before the space age [e.g., Bartels, 1950; Langeheese, 1953; Chkhetiya, 1975; Akasofu *et al.*, 1988; Hapgood, 1993; Pancheva *et al.*, 1991; Bowman, 1996; Rich *et al.*, 2003; Apostolov *et al.*, 2004; Hocke, 2008, and references therein]. The  $\sim 27$ -day solar rotation period is clearly connected with recurrent periodicity in ionospheric disturbances. Features on the Sun which cause ionospheric disturbances may produce recurrent activity if the features themselves last for more than a single solar rotation. High-speed solar wind streams (HSSs) are one phenomena which fulfil this criterion. HSSs evolve as a result of fast solar wind emitted from coronal holes on the Sun. Such "fast" wind ( $> \sim 450$  km s<sup>-1</sup>) catches up with preceding "slow" solar wind ( $\sim 300$  km s<sup>-1</sup>) and at the interface between the two a "corotating interaction region" (CIR) is formed. Thus, a single coronal hole which persists for more than one solar rotation may produce multiple CIRs and also multiple periods of fast solar wind.

This results in upstream solar wind objects such as the Earth encountering similar conditions in a repeatable fashion every 27 days (or more frequently if more than one coronal hole is present on the Sun). Figure 1 shows a schematic of this process, with the typical regions and magnetospheric responses given in Table 1 [after Borovsky and Denton, 2009a]. It should also be noted that in the literature researchers (including the present authors) have previously used the terms "CIR" and "HSS" somewhat interchangeably, referring to "CIR-driven" and/or "HSS-driven" storms or events. Strictly, the CIR which forms on the leading edge of the HSS is a region that is of limited size and duration (at Earth), and which marks the start of the prolonged period of high solar wind speed. From the point of view of the inner magnetosphere/ionosphere response, it is the long duration (days) of this high-speed solar wind which is the most salient feature of these types of events, and hence "HSS event" is used in this study as the more accurate descriptor.

[3] Work on HSS effects within the magnetosphere has accelerated during the current solar cycle [Denton *et al.*, 2008; Kavanagh and Denton, 2007] with a review of HSS-driven storms presented by Tsurutani *et al.* [2006], and detailed statistical analyses of HSSs being calculated by McPherron and Weygand [2006] and McPherron *et al.* [2009].

<sup>1</sup>Department of Communication Systems, Lancaster University, Lancaster, UK.

<sup>2</sup>Sodankylä Geophysical Observatory, Sodankylä, Finland.

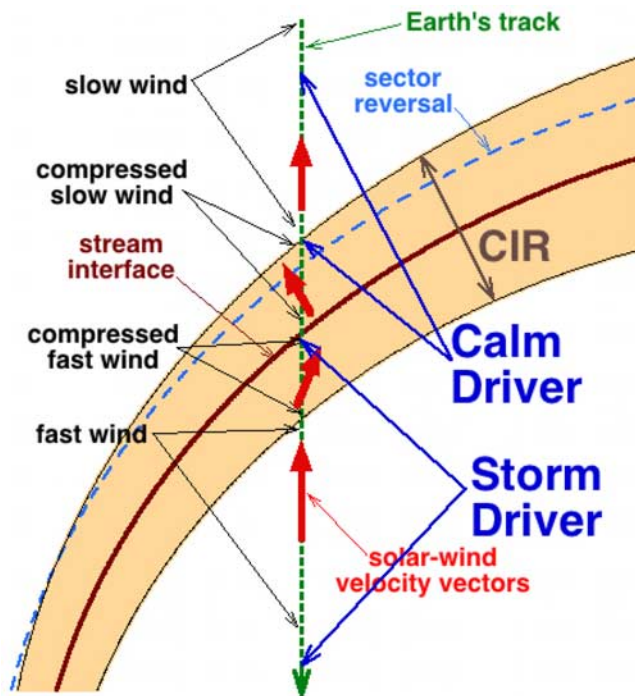


**Figure 1.** Schematic showing the structure of a typical high-speed stream (HSS), including the embedded corotating interaction region (CIR) [after Borovsky and Denton, 2009b].

Borovsky and Denton [2009a] recently presented correlations between relativistic electron dropouts at geosynchronous orbit and the occurrence of plasmaspheric drainage plumes and a superhot/superdense plasma sheet [Denton and Borovsky, 2008, 2009], with EMIC wave interactions proposed as the principal cause of relativistic electron precipitation into the atmosphere [see also MacDonald et al., 2008; Rodger et al., 2008; Sandanger et al., 2009; Summers and Thorne, 2003]. With direct relation to the ionosphere-plasmasphere system, Borovsky and Denton [2009b] have produced a detailed explanation of plasmaspheric drainage plume behavior during HSSs and carried out detailed statistical analyses of plume evolution. Such ionospheric material has direct implications for mass/energy coupling of the solar wind to the magnetosphere [Borovsky and Denton, 2006b]. For the lower thermosphere, Mlynczak et al. [2008] report a 9-day periodicity in the infrared energy budget of the thermosphere using data from SABER and SEE instruments on the NASA/TIMED satellite. This periodicity coincides with coronal holes (and associated high-speed solar wind streams) which recur with  $\sim 9$ -day frequency [Temmer et al., 2007] and are particularly strong in 2002–2006. An indication of broad density changes within the Earth's thermosphere in response to HSSs has been noted by Lei et al. [2008] and Thayer et al. [2008] who detect this same 9-day periodicity in thermospheric density using accelerometer measurements from the CHAMP satellite during 2005 and 2006.

[4] In comparing and contrasting “geomagnetic disturbances” or “storms” driven by coronal mass ejections (CMEs) with similar events driven by HSSs, it should be noted that more attention is generally given to the former since CMEs are events of shorter duration and they generally cause the largest excursions in the *Dst* and *Kp* indices. However, HSSs, simply because of their longer duration, may actually impart an equivalent (or greater) amount of energy into the Earth's magnetosphere as do CME-driven storms [Turner et al., 2006]. Indeed, HSSs are known to be of greater importance than CMEs for certain magnetospheric processes (e.g., radiation belt energization, plasma sheet temperature elevation). A general comparison between CME-driven storms and HSS-driven storms are given by Borovsky and Denton [2006a] while Denton et al. [2006] compared and contrasted average plasma sheet parameters at geosynchronous orbit during each type of storm driver and Longden et al. [2008] compared and contrasted particle precipitation rates for CME-driven and HSS-driven storms. In addition, Lindsay et al. [1995] have previously compared HSSs and CMEs characteristics during solar cycle 21 using Pioneer Venus Orbiter data while Watari [1997] used IMP-8 data to describe the broad effects of high-speed streams within the magnetosphere and emphasized the importance of the Russell-McPherron effect [Russell and McPherron, 1973] upon the coupling.

[5] Briefly, during its passage over the magnetosphere, a typical HSS will induce phenomena including the following: (1) Elevated solar wind speed lasting for many days. (2) A pulse of elevated density on the leading edge of the CIR. (3) Enhanced magnetospheric convection which persists for many days. (4) Elevated heating and higher density within the Earth's plasma sheet. (5) The possible dropout and recovery of radiation belt fluxes at geosynchronous orbit. (6) Enhanced wave-particle interactions in the inner magnetosphere. (7) Enhanced particle precipitation in the auroral regions.

[6] In this report we aim to determine the average response of parameters within the Earth's midlatitude ionosphere to this sequence of events and show that because of their repeatable nature it is possible to predict the broad response of the ionosphere on the basis of parameters measured by upstream solar wind monitors at the L1 point. It is hoped the work will allow inclusion of such knowledge within current ionospheric models, and hence improve predictions of ionospheric conditions. Also, it is hoped the results will help stimulate more accurate prediction of radio propagation effects during high-speed solar wind streams.

## 2. Data Set and Statistical Analyses

[7] HSSs are repeatable phenomena (they recur if the source region persists for more than a single solar rotation). In the current study, we perform superposed epoch analysis of ionospheric data use the same list of 124 HSS events that have successfully been used in studies of the

**Table 1.** Summary of How of Geomagnetic Activity Responds During the Passage of a High-Speed Solar Wind Stream<sup>a</sup>

| Solar Wind Properties      | Geomagnetic Response                            |
|----------------------------|---|
| Slow solar wind            | “Calm” occurs ~70% of the time                  |
| Start of CIR               | End of calm period                              |
| Compressed slow solar wind | Mild geomagnetic activity                       |
| Stream interface           | “Storm” onset and elevated geomagnetic activity |
| Compressed fast solar wind | Elevated geomagnetic activity                   |
| End of CIR                 | Elevated geomagnetic activity                   |
| Fast solar wind            | Geomagnetic activity declines over many days    |

<sup>a</sup>Geomagnetic activities include, for example, magnetospheric convection.

magnetospheric response to HSSs [Denton *et al.*, 2008, Denton and Borovsky, 2008, 2009; Borovsky and Denton, 2009a, 2009b]. In brief, the list is constructed on the basis of an initial list of CIR interfaces for 1993–1996 provided by R. McPherron (private communication, 2005). More events were added by searching solar wind data for years beyond 1996 and identifying typical signatures of HSSs (e.g., E/W flow deflection followed by sustained elevated solar wind speed). The final list of HSSs between 1993 and 2006, includes an “onset time” which is the time of convection onset following the stream interface in the solar wind. Convection onsets were initially detected following a rise in the  $Kp$  index with the final onset time at ~30 min time resolution provided by reference to the  $MBI$  (Midnight Boundary Index). Increases in  $Kp$  and  $MBI$  have been shown to be highly correlated with convection onsets [Thomsen, 2004]. It should be noted that events with no discernable increase in convection following a HSS identification in the solar wind are not included in the study. Hence, this event selection corresponds solely to events which are the most Russell-McPherron effective [Russell and McPherron, 1973; McPherron *et al.*, 2009].

[8] Figure 2 shows superposed epoch solar wind/magnetospheric parameters during the high-speed stream events used in this study from two days prior to zero epoch to four days after zero epoch (solar wind parameters are only included in the average for years beyond 1994). These data are taken from the high time resolution (1-min) OMNI2 database [King and Papitashvili, 2005] with associated other parameters. The red and blue lines indicate the upper and lower quartiles for the data, while the black solid line and the black dashed line indicate the mean and the median respectively. The gray region represents a spread of one standard deviation from the mean. Typical signatures of high-speed streams are evident in the plots which show the following:

[9] 1. A small decrease in the  $Dst$  index to around  $-20$  nT at zero epoch. The  $Dst$  index slowly increases during a prolonged recovery period lasting days.

[10] 2. A sharp increase in magnetospheric convection at zero epoch as shown by the sudden increase in the  $Kp$  index and a decrease in the Midnight Boundary Index. Such elevated convection persists for at least four days

while the “calm before the storm” [Clilverd *et al.*, 1993; Borovsky and Steinberg, 2006] is evinced by the extremely low values of  $Kp$  prior to zero epoch.

[11] 3. An increase in the overall solar wind speed ( $V$ -SW) and a west-to-east deflection in the  $y$  component of the solar wind ( $V_y$ -SW) around zero epoch.

[12] 4. An increase in the northern hemisphere Polar Cap Index (PCI) indicating increased coupling between the magnetosphere and the IMF [Troshichev *et al.*, 1988].

[13] 5. An increase in the density of the solar wind (N-SW) due to the interaction between fast and slow solar winds in the CIR. The density peaks close to zero epoch, and falls to preevent levels ~1 day after zero epoch.

[14] 6. A brief negative turning in the southward component of the interplanetary magnetic field in GSM coordinates ( $B_z$ -GSM) close to zero epoch indicating that the arrival of the HSSs being studied was accompanied by southward IMF- $B_z$  on average.

[15] 7. A nonvarying value of the F10.7 index indicating little change in the ionising solar EUV flux throughout events.

[16] To determine the effects of the events in Figure 2 upon ionospheric parameters, we perform a superposed epoch analysis of ionosonde data, initially for a single ionosonde station (Juliusruh, Germany; 54.6N, 13.4E). The results of this analysis for the F2 layer critical frequency (foF2) are shown in Figure 3. The colored traces plot the individual ionosonde measurements (where available) for the 124 events used in the analysis, while the solid black line shows the mean value of foF2 (at one hour time resolution), from eight days prior to zero epoch to sixteen days beyond zero epoch (each HSS event is plotted a different color). Data are simply binned according to epoch time, and at this stage no attempt is made to further remove the residual diurnal variation which remains evident as a quasi-sinusoidal fluctuation. It is caused by the domination of a few events with exceptionally low/high values of foF2. It is evident that in addition to this diurnal variation, there is also a step change in foF2 at the point of zero epoch (onset of convection) where a significant drop in this magnitude of this parameter occurs. During the following few days foF2 recovers to its preepoch value. It is clear that the arrival of HSSs and subsequent associated

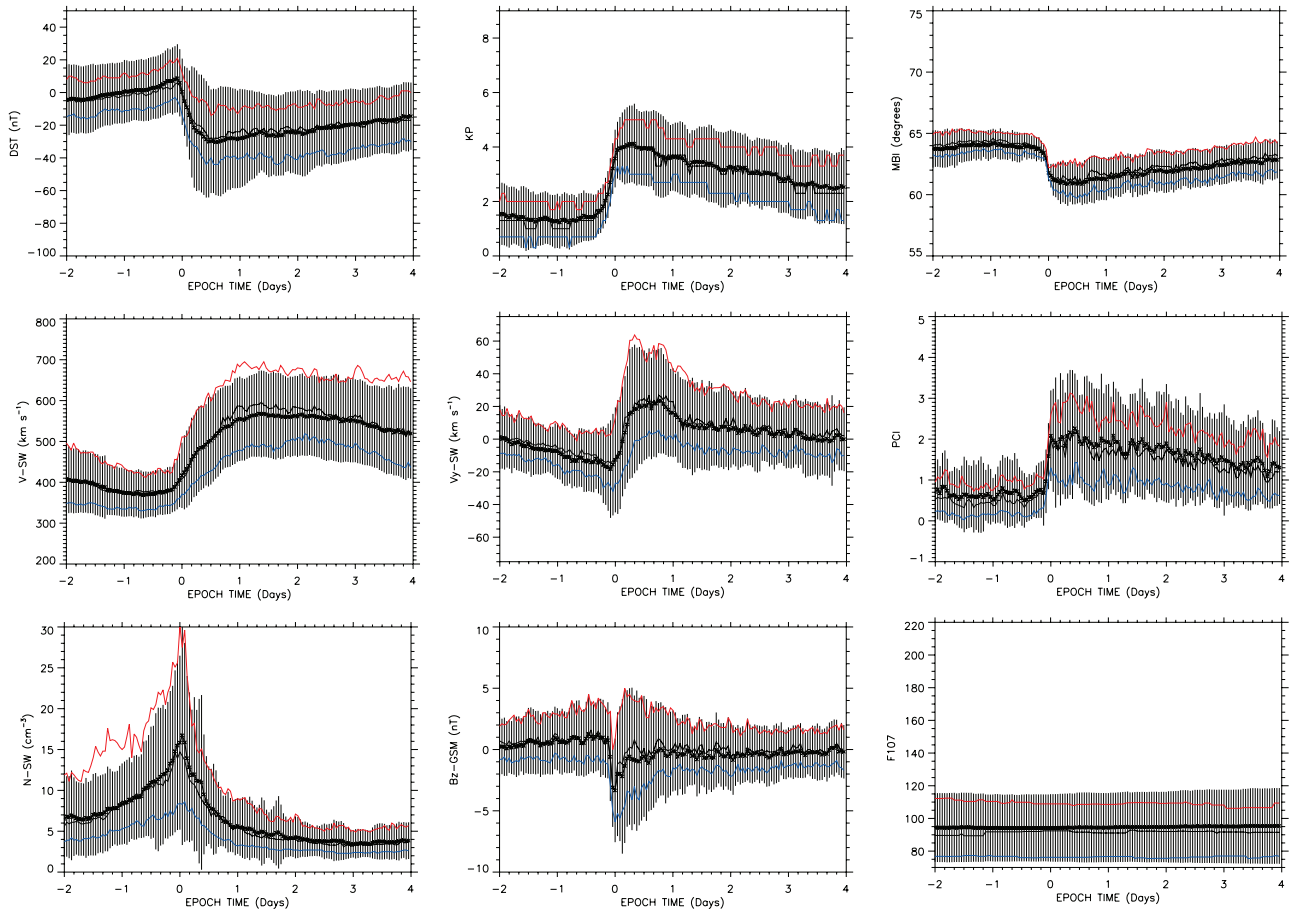


**Figure 2.** Superposed epoch plots of various solar wind, magnetospheric, and geophysical indices during 124 high-speed solar wind streams between 1993 and 2006. The variation of these indices is shown from 2 days prior to convection onset (zero epoch) to 4 days after convection onset. Typical features of HSSs are evident, including an increase in solar wind speed close to zero epoch and persistent high speed for a number of days. In addition, magnetic convection ( $Kp$  and  $MBI$ ) increases sharply and remain elevated for days. The thick black line is the mean, the thin black line is the median, and the red and blue lines are the upper and lower quartiles of the data, respectively. The gray bars indicate the region within one standard deviation of the mean for each parameter.

effects within the magnetosphere produce a clear and measurable effect in the ionosphere.

[17] The electron density at the F2 peak is directly proportional to the square of the critical frequency of the layer, namely,

$$NmF2 = 1.24(10^{10})foF2^2, \quad (1)$$

where  $NmF2$  is the number density at the F2 peak (in  $m^{-3}$ ) and  $foF2$  is critical frequency at the F2 peak (in MHz) [Piggott and Rawer, 1972]. The height of the F2 peak is usually obtained from standard ionospheric parameters

by an empirical formula. A number of such formulae have been developed over the years. The most fundamental states that height of F2 ( $hmF2$ ) is simply inversely proportional to the maximum usable frequency factor  $M(3000)F2$ , i.e., for heights in kilometers [Shimazaki, 1955]

$$hmF2 = 1490/M(3000)F2 - 176. \quad (2)$$

However, other authors noted that this formula is too crude, because it neglects the effects of retardation of the radio wave due to ionization below the F2 peak. Various other formulae try to account for this, usually by adding a correction term proportional to the ratio of critical

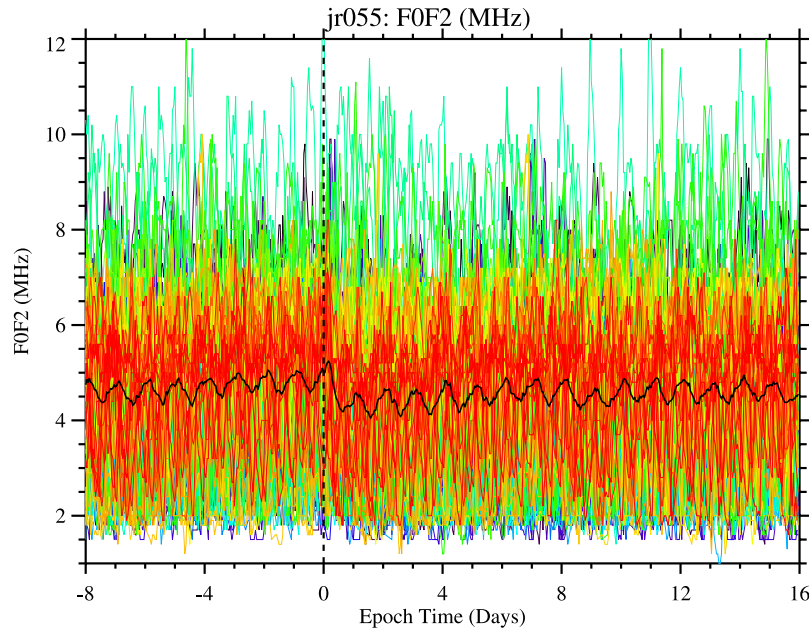


**Figure 3.** The individual (colored) and mean (black) values of the frequency of the F2 peak (foF2) measured at Juliusruh as a function of epoch time for 124 HSSs between 1993 and 2006 for 8 days prior to zero epoch to 16 days after zero epoch (1-hour time resolution). The underlying sinusoidal, diurnal variation in foF2 is clear. In addition, foF2 undergoes a sharp fall at zero epoch (convection onset) and slowly recovers to its preevent level over the next  $\sim 4$  days.

frequencies of the F2 and E layer (foF2/foE). However, Ulich [2000] found equation (56) of Dudeney [1974] to work most reliably. Hence, in all analyses below, hmF2(1) refers to the height of the F2 peak calculated from equation (2) and hmF2(2) refers to the height of the F2 peak calculated from equation 56 of Dudeney [1974].

[18] To concentrate on the actual changes associated with the stream interface and the subsequent period during the high-speed stream, Figure 4 shows averaged foF2 values and also the derived values of F2 peak density (NmF2) and height (hmF2). For clarity, the plots show the mean of each parameter (thick black line), median (thin black line), upper (red) and lower (blue) quartiles in a similar manner to Figure 2. The region within one standard deviation of the mean is indicated in gray. The most striking feature in the plot is again the diurnal variation caused by high values in these parameters from a number of the events which dominate the averages. However, several other distinct features are readily discernable. The day prior to zero epoch (prior to convection onset), the extremely low values of convection during the “calm” result in a gradual decline in average values of hmF2. Subsequently, following the onset of convection at zero epoch, a sudden decrease occurs in foF2 and results in the decrease of the calculated values of NmF2 and the increase in the calculated values of hmF2. Although a precise estimate of when all three parameters return to

“preevent” values is difficult to ascertain, it is clear that the effects of the high-speed stream in the ionosphere persist for at least four days on average.

[19] To reveal the differences between the daytime response and nighttime response to HSS arrival at the Earth’s magnetosphere, Figures 5 and 6 contain plots of equivalent analyses to those shown in Figure 4, but split between daytime (1100–0300 LT) and nighttime (2300–0300 LT), respectively. A similar analysis technique was used by Denton *et al.* [1999] to assess differences in daytime and nighttime topside ionosphere temperatures. In the current study, these local time ranges are chosen to ensure that the data in each plot are from periods when the ionosphere is largely in sunlight or darkness. Because of the large spread of data in these plots, only the mean (solid black line) and standard deviations (gray) are shown for clarity. Analysis indicates that the increase/decrease in foF2, NmF2, and hmF2, during both sunlight and darkness, is of a similar magnitude. The only noticeable difference between the two is that around the time of zero epoch, the onset of changes to the aforementioned parameters occur over a shorter timescale during the daytime than during the night (the changes in foF2, NmF2, and hmF2 are sharper during the daytime than during the night). This is likely due to the “reservoir” of plasma produced during the daytime, which then descends along flux tubes and undergoes recombination in the nighttime.

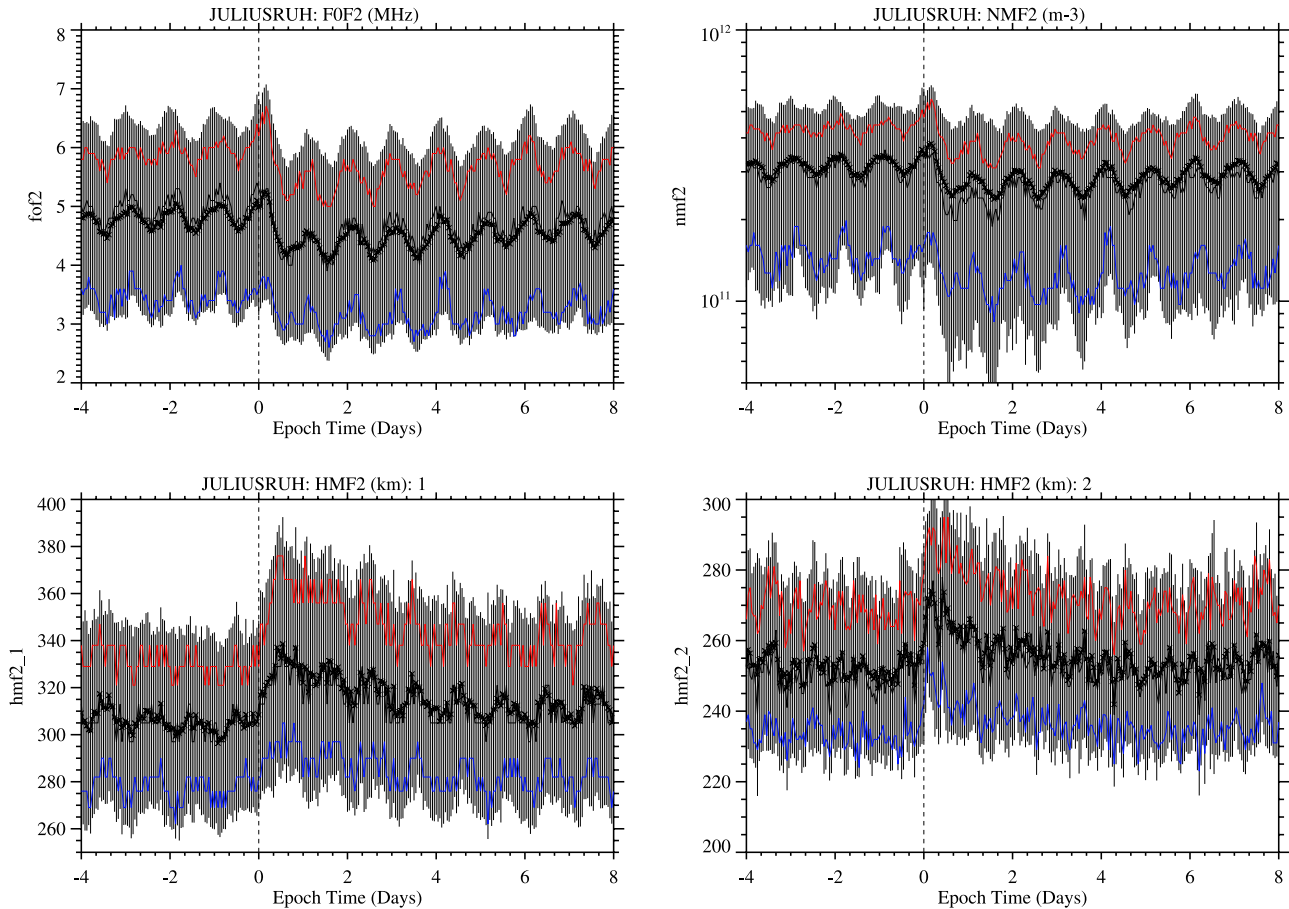


**Figure 4.** Superposed epoch plots of foF2, NmF2, and hmF2 (calculated via methods 1 and 2) for 124 HSSs between 1993 and 2006 for 4 days prior to zero epoch to 8 days after zero epoch. A step change is clear in all parameters at zero epoch (convection onset). Averaged values of foF2 and NmF2 fall while hmF2 increases. The thick black line is the mean, the thin black line is the median, and the red and blue lines are the upper and lower quartiles of the data, respectively. The gray bars indicate the region within one standard deviation of the mean.

Hence, during the nighttime this reservoir of plasma suppresses the sharp changes evident at convection onset seen in the daytime.

### 3. Discussion

[20] The broad dynamics of the midlatitude F region are largely controlled by production (e.g., solar EUV flux), transport (e.g., thermospheric winds), and loss (e.g., recombination) processes [e.g., Oliver *et al.*, 2008]. The F region is known to vary substantially between solar maximum and solar minimum and this variation may be detected in the ionosphere itself [e.g., Richards, 2001], in the topside and plasmasphere regions [e.g., Denton *et al.*, 1999] or in other regions of the magnetosphere such as the plasma sheet where ionospheric material is only a minor constituent of the overall population [e.g., Thomsen *et al.*, 2007; Chen and Moore, 2008]. Theoretical models help to

determine the principal parameters affecting the density, temperature and composition in the ionosphere and plasmasphere as a function of solar cycle [e.g., Bailey *et al.*, 2000], season [e.g., Richards, 2001], or storm driver [e.g., Denton *et al.*, 2002]. HSSs are typically solar minimum/declining phase phenomena, and the density, height, and peak frequency in the F2 layer respond primarily to the ionising EUV and X-ray fluxes, the ionising particle flux, and the behavior of thermospheric neutral winds. The expected behavior of the density at the F2 peak during an “F region ionospheric storm” mirrors that of the *Dst* index during a traditional magnetospheric storm [e.g., Hargreaves, 1992; Buonsanto, 1999]. The average NmF2 initially falls during such a storm and the entire F region broadens during the “main phase” and then enters a “recovery period” over a period of one to several days.

[21] The most reasonable explanation for the results shown in Figures 3–6 is the onset of ionospheric F region

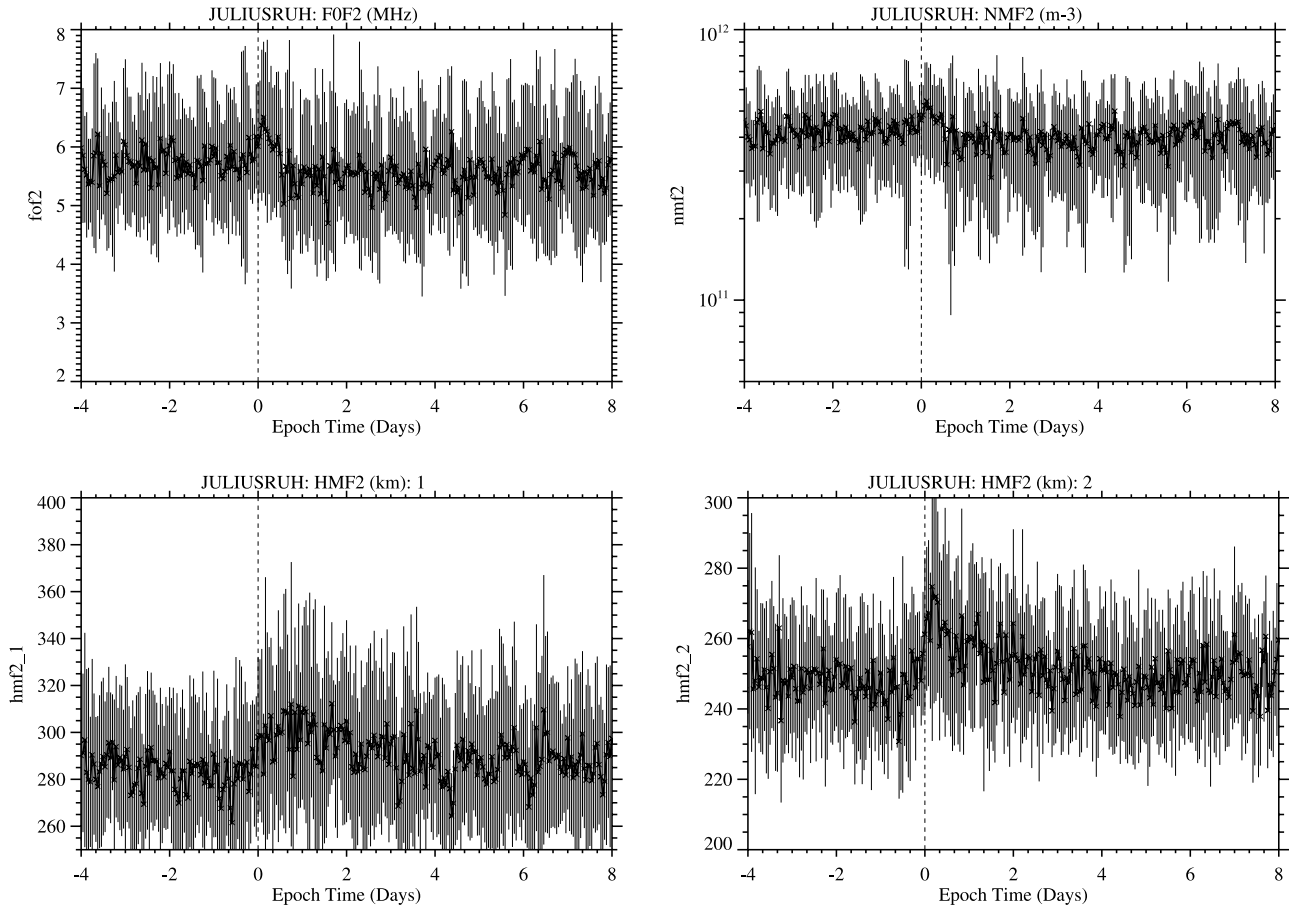


**Figure 5.** Superposed epoch plots of the daytime (1100–1500 LT) foF2, NmF2, and hmF2 (calculated via methods 1 and 2) for 124 HSSs between 1993 and 2006 for 4 days prior to zero epoch to 8 days after zero epoch.

storms during HSSs (for a review of F region storms see *Buonsanto* [1999]). Such storms produce an increase in heating of the ionosphere at convection onset, caused by enhanced particle precipitation rates. Precipitation is known to be significantly enhanced during CME events and for a longer duration during HSS events [*Longden et al.*, 2008]. Changes in EUV flux can be ruled out as the cause of the change in F region parameters during HSSs because of the flat profile of the F10.7 index (see Figure 2). Hence, it seems likely that the increase in particle precipitation at high latitude during HSSs leads to an increase in ionospheric temperature which in turn increases the recombination rate; the overall result is a decrease in the density at the F2 peak [e.g., *Hargreaves*, 1992]. Also, this increase in precipitation occurs in combination with changes in thermospheric neutral wind circulation known to occur during enhanced convection and which are predicted to elevate the ionosphere [e.g., *Roble*, 1977; *Buonsanto*, 1999]. However, as noted by *Hargreaves* [1992], several explanations have been proposed for explaining the F region storm, and a comprehensive discussion of

these is beyond the scope of the current paper. Still, it should be noted that the F region does not respond to HSSs in isolation. Because of the coupled nature of the thermosphere-ionosphere-magnetosphere system, phenomena such as drainage plume dynamics [e.g., *Borovsky and Denton*, 2006b, 2009a, 2009b], refilling of the depleted outer plasmasphere [e.g., *Sandel and Denton*, 2007], the effectiveness of coupling between the solar wind and the magnetosphere [e.g., *Russell and McPherron*, 1973], and numerous other processes are all likely to play a part in production/loss, heating/cooling, and transport processes within the F region ionosphere.

[22] From the point of view of predicting the behavior of the ionosphere, the results presented above demonstrate the response of the ionosphere is repeatable and should be, to some degree, predictable during HSSs. The values of foF2, NmF2 and hmF2 all vary within narrow bands which have been well characterized in a statistical manner. Since the characteristics of HSSs in the solar wind are readily apparent, then predicting the real-time ionospheric response following a particular high-speed stream

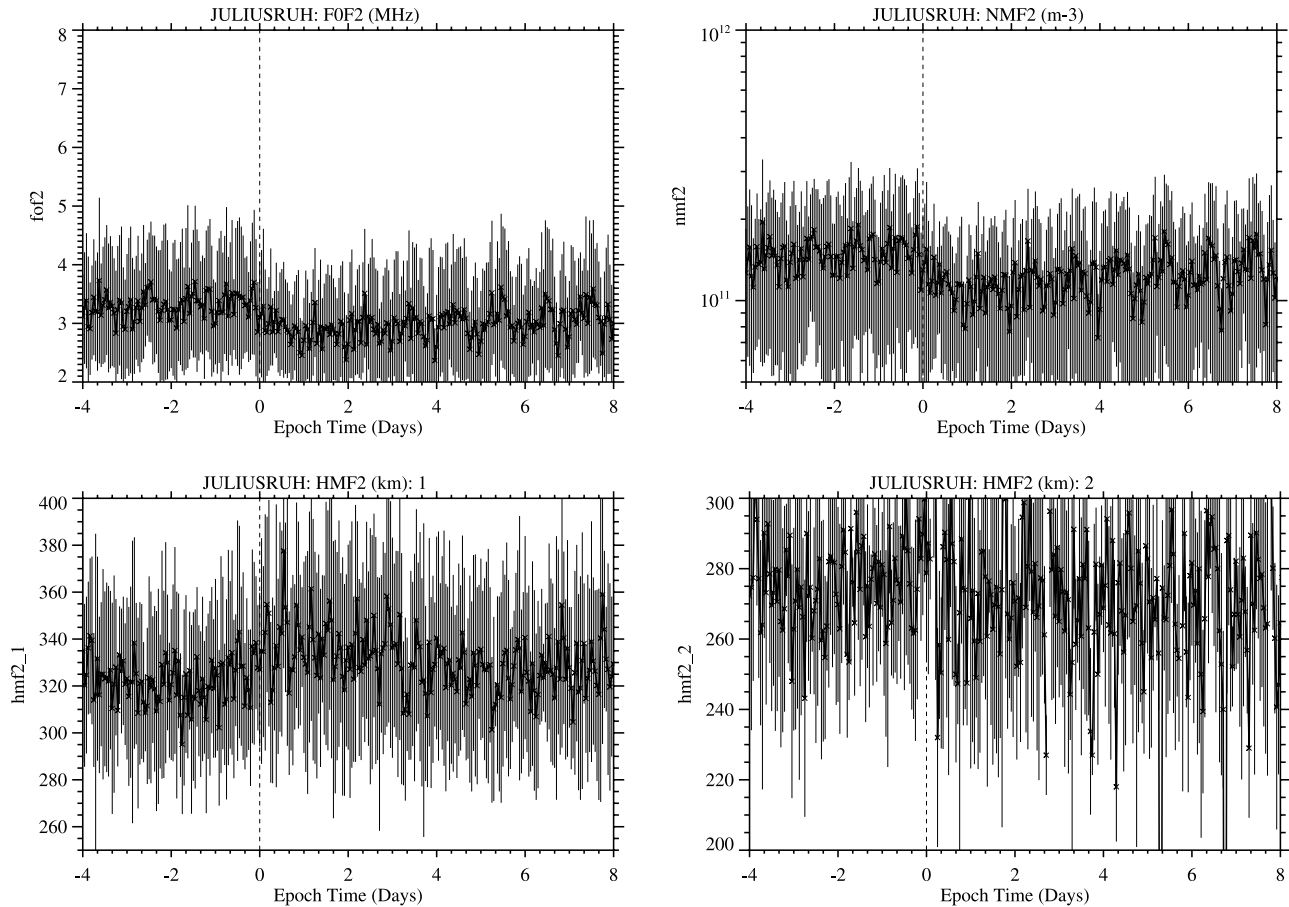


**Figure 6.** Superposed epoch plots of the nighttime (2300–0300 LT) foF2, NmF2, and hmF2 (calculated via methods 1 and 2) for 124 HSSs between 1993 and 2006 for 4 days prior to zero epoch to 8 days after zero epoch.

would rely on accurate identification of HSS signatures at some point upstream of the Earth (e.g., by a solar wind monitor such as ACE). This would lead directly to a predictive capability for ionospheric parameters which would be of use in a number of space-weather-type applications (e.g., predicting the characteristic frequencies for radio propagation). One could foresee that predictions of the ionospheric conditions for radio propagation would then be directly linked to detection of HSSs at the L1 point, upstream of the Earth.

#### 4. Conclusions and Future Work

[23] In conclusion, we note the following salient points regarding the implications for the midlatitude ionosphere of high-speed solar wind streams incident on the Earth's magnetosphere:

[24] 1. On average, HSSs cause a sharp decrease in foF2 and NmF2 which begins at the onset of magnetospheric convection. These decreases are consistent with onset of an F region ionospheric storm.

[25] 2. On average, HSSs cause an increase of  $\sim 20$  km in the peak height of the midlatitude F2 layer following convection onset.

[26] 3. On average, excursions in foF2, NmF2 and hmF2 values within the midlatitude ionosphere last for at least 4 days, gradually returning to preevent levels following event onset.

[27] It is planned to extend the work carried out in this study to include ionosonde data from other stations and thus test whether the above conclusions hold true for the ionosphere at varying latitude and longitude.

[28] **Acknowledgments.** This work was funded under the EU LAPBIAT II project and the authors gratefully acknowledge this support. We thank everyone who contributed to the Juliusruh ionosonde data set used in this study and thank Richard Stamper at Rutherford Appleton Laboratory (RAL), UK, for providing us with the data. We thank the World Data Centre, C1 at RAL for the geomagnetic indices. We also thank the U.S. Air Force Research Laboratory, Hanscom Air Force Base, Massachusetts, for providing the Midnight Boundary

Index and the Danish Meteorological Institute for the Polar Cap Index. We are grateful to Robert McPherron for providing the initial list of CIR interfaces and for useful discussions of HSSs and their magnetospheric consequences. M.D. would like to thank the Sodankylä Geophysical Observatory for their hospitality during his visit in April 2008 and would also like to thank Michelle Thomsen and others in the ISR-1 group at Los Alamos National Laboratory for many extremely useful discussions related to high-speed solar wind streams and magnetospheric physics in general. M.D. would especially like to thank Joe Borovsky at LANL for insightful comments and suggestions in the preparation of this manuscript.

## References

- Akasofu, S. I., C. Olmsted, T. Saito, and T. Oki (1988), Quantitative forecasting of the 27-day recurrent magnetic activity, *Planet. Space Sci.*, *36*, 1133–1147, doi:10.1016/0032-0633(88)90068-2.
- Apostolov, E. M., D. Altadill, and M. Todorova (2004), The 22-year cycle in the geomagnetic 27-day recurrences reflecting on the F2-layer ionization, *Ann. Geophys.*, *22*, 1171–1176.
- Bailey, G. J., M. H. Denton, R. A. Heelis, and S. Venkatraman (2000), A modelling study of the latitudinal variations in the nighttime plasma temperatures of the equatorial topside ionosphere during northern winter at solar maximum, *Ann. Geophys.*, *18*, 1435–1446, doi:10.1007/s00585-000-1435-6.
- Bartels, J. (1950), 27-day variations in the F2 layer critical frequencies at Huancayo, *J. Atmos. Terr. Phys.*, *1*, 2–12, doi:10.1016/0021-9169(50)90010-9.
- Borovsky, J. E., and M. H. Denton (2006a), Differences between CME-driven storms and CIR-driven storms, *J. Geophys. Res.*, *111*, A07S08, doi:10.1029/2005JA011447.
- Borovsky, J. E., and M. H. Denton (2006b), The effect of plasmaspheric drainage plumes on solar-wind/magnetosphere coupling, *Geophys. Res. Lett.*, *33*, L20101, doi:10.1029/2006GL026519.
- Borovsky, J. E., and M. H. Denton (2009a), A statistical look at plasmaspheric drainage plumes, *J. Geophys. Res.*, *113*, A09221, doi:10.1029/2007JA012994.
- Borovsky, J. E., and M. H. Denton (2009b), Relativistic-electron dropouts and recovery: A superposed epoch study of the magnetosphere and the solar wind, *J. Geophys. Res.*, *114*, A02201, doi:10.1029/2008JA013128.
- Borovsky, J. E., and J. T. Steinberg (2006), The “calm before the storm” in CIR/magnetosphere interactions: Occurrence statistics, solar wind statistics, and magnetospheric preconditioning, *J. Geophys. Res.*, *111*, A07S10, doi:10.1029/2005JA011397.
- Bowman, G. G. (1996), The influence of the 27-day variation in the upper atmosphere neutral-particle density on ionospheric spread-F occurrence, *J. Geomag. Geoelectr.*, *48*, 1043–1057.
- Buonsanto, M. J. (1999), Ionospheric storms: A review, *Space Sci. Rev.*, *88*, 563–601, doi:10.1023/A:1005107532631.
- Chen, S.-H., and T. E. Moore (2008), Ionospheric ions in the near-Earth magnetotail, *J. Geophys. Res.*, *113*, A08232, doi:10.1029/2007JA012816.
- Chkhetiya, A. M. (1975), Planetary distribution of 27-day variation of electron concentration in maximum of F-layer of ionosphere, *Geomagn. Aeron.*, *15*, 160–161.
- Cliiverd, M. A., T. D. G. Clark, A. J. Smith, and N. R. Thomson (1993), Observation of a decrease in mid-latitude whistler mode signal occurrence prior to geomagnetic storms, *J. Atmos. Terr. Phys.*, *55*(10), 1479–1485, doi:10.1016/0021-9169(93)90113-D.
- Denton, M. H., and J. E. Borovsky (2008), Superposed epoch analysis of high-speed-stream effects at geosynchronous orbit: Hot plasma, cold plasma, and the solar wind, *J. Geophys. Res.*, *113*, A07216, doi:10.1029/2007JA012998.
- Denton, M. H., and J. E. Borovsky (2009), The superdense plasma sheet in the magnetosphere during high-speed-stream-driven storms: Plasma transport and timescales, *J. Atmos. Sol. Terr. Phys.*, in press.
- Denton, M. H., G. J. Bailey, Y. Z. Su, K.-I. Oyama, and T. Abe (1999), High altitude observations of electron temperature and a possible north/south asymmetry, *J. Atmos. Sol. Terr. Phys.*, *61*, 775–788.
- Denton, M. H., G. J. Bailey, C. R. Wilford, A. S. Rodger, and S. Venkatraman (2002), He<sup>+</sup> dominance in the plasmasphere during geomagnetically disturbed periods: Part 1. Observational results, *Ann. Geophys.*, *20*, 461–470.
- Denton, M. H., J. E. Borovsky, R. M. Skoug, M. F. Thomsen, B. Lavraud, M. G. Henderson, R. L. McPherron, J. C. Zhang, and M. W. Liemohn (2006), Geomagnetic storms driven by ICME- and CIR-dominated solar wind, *J. Geophys. Res.*, *111*, A07S07, doi:10.1029/2005JA011436.
- Denton, M. H., J. E. Borovsky, R. B. Horne, R. L. McPherron, S. K. Morley, and B. T. Tsurutani (2008), High speed solar wind streams: A call for key research, *Eos Trans. AGU*, *89*(7), 62–63, doi:10.1029/2008EO070002.
- Dudeney, J. R. (1974), A simple empirical method for estimating the height and semi-thickness of the F2-layer at the Argentine Islands, Graham Land, *Sci. Rep.* *88*, Br. Antarct. Surv., Cambridge, U. K.
- Hapgood, M. A. (1993), A double solar-cycle in the 27-day recurrence of geomagnetic activity, *Ann. Geophys.*, *11*, 248–253.
- Hargreaves, J. K. (1992), *The Solar-Terrestrial Environment: An Introduction to Geospace---The Science of the Terrestrial Upper Atmosphere, Ionosphere, and Magnetosphere*, Cambridge Univ. Press, Cambridge, U. K.
- Hocke, K. (2008), Oscillations of global mean TEC, *J. Geophys. Res.*, *113*, A04302, doi:10.1029/2007JA012798.
- Kavanagh, A., and M. H. Denton (2007), High speed solar wind streams and geospace interactions, *Astron. Geophys.*, *48*, 6.24–6.26.
- King, J. H., and N. E. Papitashvili (2005), Solar wind spatial scales in and comparisons of hourly Wind and ACE plasma and magnetic field data, *J. Geophys. Res.*, *110*, A02104, doi:10.1029/2004JA010649.
- Langehesse, G. (1953), 27 day variations in the absorption of the D-region of the ionosphere over Singapore and Slough, *J. Atmos. Terr. Phys.*, *3*, 153–162, doi:10.1016/0021-9169(53)90101-9.
- Lei, J., J. P. Thayer, J. M. Forbes, E. K. Sutton, and R. S. Nerem (2008), Rotating solar coronal holes and periodic modulation of the upper atmosphere, *Geophys. Res. Lett.*, *35*, L10109, doi:10.1029/2008GL033875.
- Lindsay, G. M., C. T. Russell, and J. G. Luhmann (1995), Coronal mass ejections and stream interaction region characteristics and their potential geomagnetic consequences, *J. Geophys. Res.*, *100*, 16,999–17,013, doi:10.1029/95JA00525.
- Longden, N., M. H. Denton, and F. Honary (2008), Particle precipitation during ICME-driven and CIR-driven geomagnetic storms, *J. Geophys. Res.*, *113*, A06205, doi:10.1029/2007JA012752.
- MacDonald, E. A., M. H. Denton, M. F. Thomsen, and S. P. Gary (2008), Superposed epoch analysis of a whistler instability criterion at geosynchronous orbit during geomagnetic storms, *J. Atmos. Sol. Terr. Phys.*, *70*, 1789–1796, doi:10.1016/j.jastp.2008.03.021.
- McPherron, R. L., and J. Weygand (2006), The solar wind and geomagnetic activity as a function of time relative to corotating interaction regions, in *Recurrent Geomagnetic Storms: Corotating Solar Wind Streams*, *Geophys. Monogr. Ser.*, vol. 167, edited by B. T. Tsurutani et al., pp. 125–137, AGU, Washington, D. C.
- McPherron, R. L., D. N. Baker, and N. U. Crooker (2009), Role of the Russell-McPherron effect in the acceleration of relativistic electrons, *J. Atmos. Sol. Terr. Phys.*, in press.
- Mlynczak, M. G., F. J. Martin-Torres, C. J. Mertens, B. T. Marshall, R. E. Thompson, J. U. Kozyra, E. E. Remsburg, L. L. Gordley, J. M. Russell III, and T. Woods (2008), Solar-terrestrial coupling evidenced by periodic behavior in geomagnetic indexes and the infrared energy budget of the thermosphere, *Geophys. Res. Lett.*, *35*, L05808, doi:10.1029/2007GL032620.
- Oliver, W. L., S. Kawamura, and S. Fukao (2008), The causes of mid-latitude F Layer behavior, *J. Geophys. Res.*, *113*, A08310, doi:10.1029/2007JA012590.
- Pancheva, D., R. Schminder, and J. Lastovicka (1991), 27-day fluctuations in the ionospheric D-region, *J. Atmos. Terr. Phys.*, *53*, 1145–1150, doi:10.1016/0021-9169(91)90064-E.
- Piggott, W. R., and K. Rawer (Eds.) (1972), *URSI Handbook of Ionogram Interpretation and Reduction*, 2nd ed., NOAA, Asheville, N. C.

- Rich, F. J., P. J. Sultan, and W. J. Burke (2003), The 27-day variations of plasma densities and temperatures in the topside ionosphere, *J. Geophys. Res.*, *108*(A7), 1297, doi:10.1029/2002JA009731.
- Richards, P. G. (2001), Seasonal and solar cycle variations of the ionospheric peak electron density: Comparison of measurement and models, *J. Geophys. Res.*, *106*, 12,803–12,819, doi:10.1029/2000JA000365.
- Roble, R. G. (1977), *The Upper Atmosphere and Magnetosphere*, Natl. Acad. of Sci., Washington, D. C.
- Rodger, C. J., T. Raita, M. A. Clilverd, A. Seppälä, S. Dietrich, N. R. Thomsen, and T. Ulich (2008), Observations of relativistic electron precipitation from the radiation belts driven by EMIC waves, *Geophys. Res. Lett.*, *35*, L16106, doi:10.1029/2008GL034804.
- Russell, C. T., and R. L. McPherron (1973), Semiannual variation of geomagnetic activity, *J. Geophys. Res.*, *78*, 92–108, doi:10.1029/JA078i001p00092.
- Sandanger, M. I. J., F. Søråas, M. Sørbø, K. Aarsnes, K. Oksavik, and D. S. Evans (2009), Relativistic electron losses related to EMIC waves during CIR and CME storms, *J. Atmos. Sol. Terr. Phys.*, doi:10.1016/j.jastp.2008.07.006, in press.
- Sandel, B. R., and M. H. Denton (2007), Global view of refilling of the plasmasphere, *Geophys. Res. Lett.*, *34*, L17102, doi:10.1029/2007GL030669.
- Shimazaki, T. (1955), World-wide variations in the height of the maximum electron density of the ionospheric F2 layer, *J. Radio Res. Lab. Jpn.*, *2*, 85–97.
- Summers, D., and R. M. Thorne (2003), Relativistic electron pitch-angle scattering by electromagnetic ion cyclotron waves during geomagnetic storms, *J. Geophys. Res.*, *108*(A4), 1143, doi:10.1029/2002JA009489.
- Temmer, M., B. Vršnak, and A. M. Veronig (2007), Periodic appearance of coronal holes and the related variation of solar wind parameters, *Sol. Phys.*, *241*, 371–383, doi:10.1007/s11207-007-0336-1.
- Thayer, J. P., J. Lei, J. M. Forbes, E. K. Sutton, and R. S. Nerem (2008), Thermospheric density oscillations due to periodic solar wind high-speed streams, *J. Geophys. Res.*, *113*, A06307, doi:10.1029/2008JA013190.
- Thomsen, M. F. (2004), Why  $K_p$  is such a good measure of magnetospheric convection, *Space Weather*, *2*, S11004, doi:10.1029/2004SW000089.
- Thomsen, M. F., M. H. Denton, B. Lavraud, and M. Bodeau (2007), Statistics of plasma fluxes at geosynchronous orbit over more than a full solar cycle, *Space Weather*, *5*, S03004, doi:10.1029/2006SW000257.
- Troshichev, O. A., V. G. Andrezen, S. Vennerstrøm, and E. Friis-Christensen (1988), Magnetic activity in the polar cap: A new index, *Planet. Space Sci.*, *36*, 1095–1102, doi:10.1016/0032-0633(88)90063-3.
- Tsurutani, B. T., et al. (2006), Corotating solar wind streams and recurrent geomagnetic activity: A review, *J. Geophys. Res.*, *111*, A07S01, doi:10.1029/2005JA011273.
- Turner, N. E., E. J. Mitchell, D. J. Knipp, and B. A. Emery (2006), Energetics of magnetic storms driven by corotating interaction regions: A study of geoeffectiveness, in *Recurrent Geomagnetic Storms: Corotating Solar Wind Streams*, *Geophys. Monogr. Ser.*, vol. 167, edited by B. T. Tsurutani et al., pp. 113–124, AGU, Washington, D. C.
- Ulich, T. (2000), Solar variability and long-term trends in the ionosphere, Ph.D. thesis, Oulu Univ. Press, Oulu, Finland.
- Watari, S. (1997), The effect of the high-speed stream following the corotating interaction region on the geomagnetic activities, *Ann. Geophys.*, *15*, 662–670, doi:10.1007/s00585-997-0662-5.

---

M. H. Denton, Department of Communication Systems, Lancaster University, Lancaster LA1 4WA, UK. (m.denton@lancaster.ac.uk)  
 E. Turunen and T. Ulich, Sodankylä Geophysical Observatory, Tähteläntie 62, FIN-99600 Sodankylä, Finland.